

# $\mu$ Tugs: Enabling Microrobots to Deliver Macro Forces with Controllable Adhesives

David L. Christensen\*, Elliot W. Hawkes\*, Srinivasan A. Suresh, Karen Ladenheim, and Mark R. Cutkosky

**Abstract**—The controllable adhesives used by insects to both carry large loads and move quickly despite their small scale inspires the  $\mu$ Tug robot concept. These are small robots that can both move quickly and use controllable adhesion to apply interaction forces many times their body weight. The adhesives enable these autonomous robots to accomplish this feat on a variety of common surfaces without complex infrastructure. The benefits, requirements, and theoretical efficiency of the adhesive in this application are discussed as well as the practical choices of actuator and robot working surface material selection. A robot actuated by piezoelectric bimorphs demonstrates fast walking with a no-load rate of 50 Hz and a loaded rate of 10 Hz. A 12 g shape memory alloy (SMA) actuated robot demonstrates the ability to load more of the adhesive enabling it to tow 6.5 kg on glass (or 500 times its body weight). Continuous rotation actuators (electromagnetic in this case) are demonstrated on another 12 g robot give it nearly unlimited work cycles through gearing. This leads to advantages in towing capacity (up to 22 kg or over 1800 times its body weight), step size, and efficiency. This work shows that using such an adhesive system enables small robots to provide truly human scale interaction forces, despite their size and mass. This will enable future microrobots to not only sense the state of the human environment in which they operate, but apply large enough forces to modify it in response.

## I. INTRODUCTION

There are numerous impressive micro-robots [1]–[7], but many require powered external infrastructure (e.g. large electromagnets [1,2], surfaces with local magnetic fields [3], capacitive electrode surfaces [4]) or similar provisions, and even so can apply only minute interaction forces with their environments. In contrast, insects such as weaver ants (Fig. 1, left) have no required infrastructure, yet can exert substantial forces when normalized to bodyweight.

At small scales, insects exploit interaction forces like adhesion that, unlike coulomb friction, scale with area and do not depend on the magnitude of a normal force. There are many examples of insects that use adhesive pads, scopulae, and other microscopic features to attach to surfaces [8,9]; with these features, insects can apply interaction forces many times their body weight.

However, adhesion without a method of release is not useful; an insect or robot would become stuck and could not move. This problem has been reported for both small robots [10] and moving MEMS devices [11]. In addition, at smaller scales, legged locomotion requires higher step rates than at larger scales to maintain the same absolute velocity. Therefore, adhesives must engage and disengage

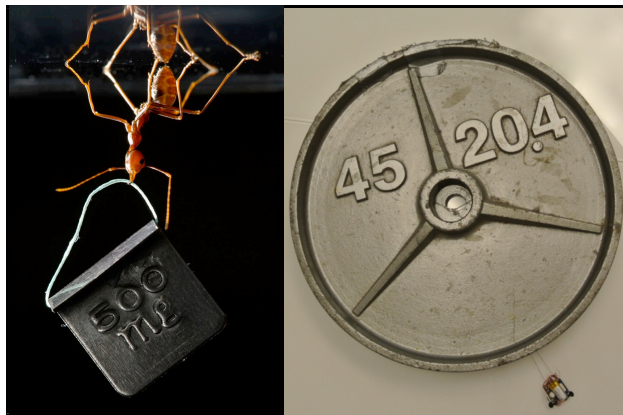


Fig. 1: Asian Weaver Ant holds 500 mg weight on an inverted surface using controllable adhesion (left, image courtesy of T. Endlein, Cambridge). The 12 g  $\mu$ Tug robot (visible at lower right) uses controllable adhesion to tow over 20 kg on smooth surfaces.

more quickly at small scales. To allow easy and fast release of adhesion, an insect or microrobot needs a *controllable adhesive* that can be activated for applying large interaction forces when required, and deactivated for locomotion with low energy expenditure. Indeed, most insects that use various forms of adhesive pads have controllable adhesion [12,13].

We use these insights as the basis for  $\mu$ Tug robots, small robots that can move easily and can apply interaction forces orders of magnitude larger than their weights. The robots employ a controllable dry adhesive that functions on a variety of smooth surfaces and allows both large force generation and high step rates, enabling the microrobots to interact with human scale environments. We discuss scaling principles and the constraints (e.g., regarding stride length and attachment/detachment work per cycle) that apply to this class of miniature robot and demonstrate the principles for  $\mu$ Tugs towing large weights. The measured performance matches predictions and illustrates some of the tradeoffs associated with different types of actuation.

Three robots are built to demonstrate some of the possibilities and challenges of the concept:

- 1) a piezoelectric bimorph based  $\mu$ Tug that demonstrates the speed capability of the controllable adhesive system
- 2) an SMA based  $\mu$ Tug that demonstrates the force generation capabilities of the adhesive system
- 3) a motor based  $\mu$ Tug that demonstrates the advantage of very large work cycles.

Finally we conclude that with proper understanding of the

\* These authors contributed equally.

All authors are with the Dept. of Mechanical Engineering, Stanford University, Stanford, CA 94305, USA DavidC10@stanford.edu

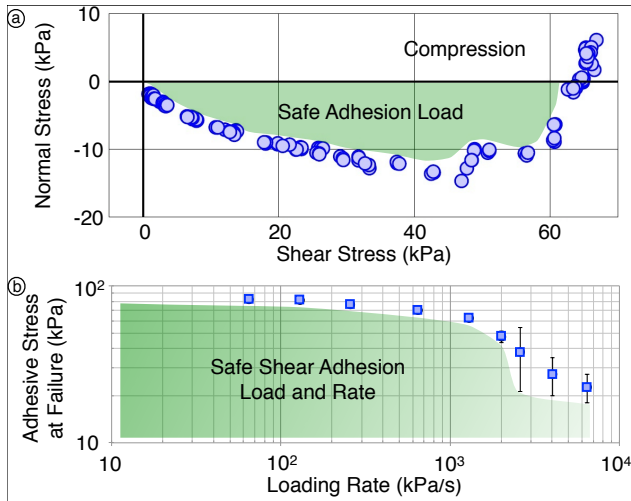


Fig. 2: a) Shows the limit curve of safe normal and shear stresses for the directional adhesives. b) Bandwidth over which the adhesives are able to provide useful levels of adhesion. Rolloff at the corner frequency is quite sharp, and small experimental variance produces a larger uncertainty in the failure stress beyond this point.

adhesive system and actuator characteristics, these 12 g or less robots are able to apply enough force to substantially interact with the human world, while still being surprisingly efficient and fast.

## II. ADHESIVES

### A. Force Generation

The dry adhesives used for this work [14,15] generate adhesion using van der Waals interactions [16] at densely arrayed contact sites. The adhesive is composed of a series of  $100\ \mu\text{m}$  wedges made of silicone rubber (Dow Corning Sylgard 170). When placed on a surface, the wedges only make contact with their tips, with a very small area of contact. When the adhesives are loaded in shear, the wedges bend over to contact the surface on their sides. This deformation increases the real area of contact and gives the system more adhesive capability. When the shear force is removed, the wedges return to their original shape, disengaging the adhesive. We define such an adhesive as directional and controllable: the adhesion is controlled by an externally applied shear load. There have been many adhesive designs that are directional and could be possibly used for miniature tugging robots [17]–[19], but because they are not controllable through shear load, would require alternative methods to turn on and off.

Once engaged, the adhesive can generate an adhesive stress in both the normal (15 kPa) and shear directions (70 kPa in the preferred direction). Fig. 2a shows the limit curve for this adhesive, indicating the magnitude of combined shear and normal pressure the adhesive can support on glass.

The key advantage of using this type of adhesive is that the available shear force does not require a normal load. A

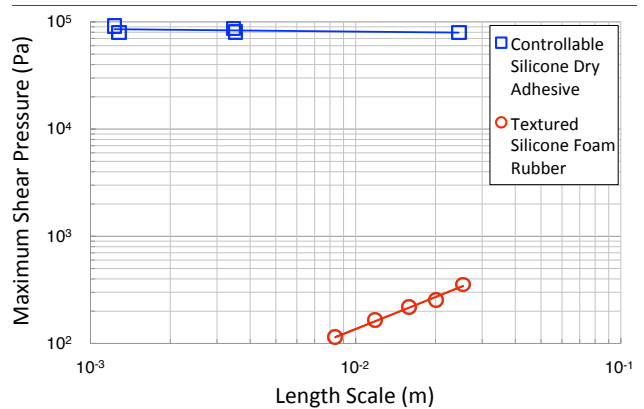


Fig. 3: Maximum shear stress while scaling a simple 25 mm silicone rubber cube (red), and an equally sized cube with a dry adhesive (blue). Note that while the available shear force decreases with robot size (with a scaling fit of  $A^{0.977}$ ), dry adhesives give constant shear stress (with a scaling fit of  $A^{-0.024}$ ). Data are from pull tests on glass.

robot using friction has a peak force limited by  $\mu \cdot mg$ , which scales as the length cubed. Adhesion, in contrast, scales only as the contact area, or length squared. This means that using an adhesive to generate ground reaction forces becomes advantageous at small size scales as shown in Fig. 3, which compares pull test data against glass, taken for small cubes of dense silicone rubber foam versus a foam cube of the same size with a dry adhesive patch on its lower surface.

### B. Cycle Speed

While traditional pressure sensitive adhesives would work well for generating ground reaction forces, detachment presents a problem. Tape peeling is a slow process; the peel propagates from one end to the other, taking significant time and mechanical work.

The fibrillar adhesive used in this paper accelerates this process by parallelizing it; each microwedge is a peeling zone so that detachment is rapid. Tests with controlled shear forces and measured adhesive forces show that the adhesive can release from 80% of full load with a time constant of approximately 9 ms. Similarly, engagement occurs in parallel over many wedges, and therefore can be fast. Fig. 2b shows the maximum supported shear stress vs loading rate characteristics of the adhesive, and shows that the performance only begins to drop off around 1 MPa/s. Combining the release time and engagement rate we get a minimum cycle time to 80% load of 77 ms, which is a combined cycle rate of 13 Hz. This is comparable to the 15 Hz stride frequency of the 2 g gecko tested in [20] whose natural adhesive system originally inspired the design of these controllable adhesives. Because the adhesion is controlled by the applied shear, the amount of adhesion will only be the amount required for a task, and lightly loaded adhesives will therefore operate at a faster overall rate.

Finally, since the adhesive is controlled by the applied shear load, engagement and disengagement can be synchronized to the gait of a robot. If done correctly, this

alleviates the need for a release actuator or careful phasing of the engagement and peeling processes that would be necessary to achieve a high step rate with an active adhesive disengagement system.

### C. Engagement Work

While the benefits of a controllable, directional fibrillar adhesive are useful, they also come with a cost. Adhesion is an energetically favorable state, and disengaging adhesion requires work. The adhesive used here uses spring energy stored in the wedges to disengage; this energy is added to the system in the process of engaging the adhesive. This mechanism has the advantage of only requiring one actuator, as the force required to engage the adhesives is in the loading direction.

The quasi-static thermodynamic energy of adhesion for bulk PDMS is  $0.047 \text{ mJ/m}^2$ . However, even at  $70 \mu\text{m/s}$ , the work required for peeling at an angle of  $40^\circ$  is  $0.2 \text{ J/m}^2$  [21]. To disengage the adhesives controllably and quickly upon release (much faster than  $70 \mu\text{m/s}$ ), there must be substantially more energy contained within the springs than the minimum required for quasi-static disengagement [21]. In the case of this adhesive, that energy is about  $3 \text{ J/m}^2$ .

Fig. 4 region (a) shows the force-displacement profile for a  $25 \text{ mm}$  square patch of adhesives (assuming the force displacement curve to be linear). This represents the minimum spring energy necessary for the system to operate at full load. Any real system will have additional springs that will be loaded and other losses, but the adhesives themselves need at least this force and displacement to function at maximum capacity. Therefore a robot that *fully* uses this adhesive must have at least this work available per cycle in its actuators to engage and disengage the adhesion. As with insects, the work required per cycle reduces with decreased loading because the adhesive only engages the amount necessary to support the load.

## III. PRACTICAL CONSIDERATIONS

### A. Working Surface Selection

The choice of working surface material presents a unique opportunity to maximize the effective impact of the adhesive robot. While choosing a material on which the adhesive performs well is obvious, it is this measure combined with the force required to move the payload that matters.

At the limit of function, the maximum adhesive shear force,  $F_s$ , on the proposed work surface will equal the friction of the maximum druggable payload or  $F_p$ . For a stainless steel payload,

$$F_s = F_p = \mu_{ss} m_p g \quad (1)$$

where  $\mu_{ss}$  is the coefficient of friction for the payload on the work surface,  $m_p$  is the mass of the payload in kg, and  $g$  is the acceleration due to gravity in  $\text{m/s}^2$ . We define a normalized performance metric as:

$$\frac{m_p}{m_r} = \frac{F_s}{\mu_{ss} \cdot m_r g} \quad (2)$$

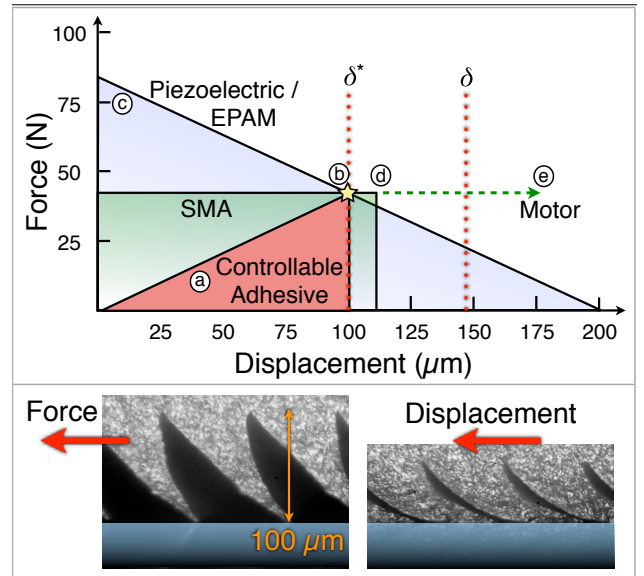


Fig. 4: Top: (a) Required work for loading  $25 \text{ mm}$  square adhesive. Due to actuator force-displacement shape mismatch, piezoelectric and EPAM actuators (c) require a stated work cycle capability of at least four times this minimum value to achieve full engagement (b). SMA (d) and motors (e) are a better match, only wasting half of their work cycle specification, up to the star symbol at center. Unused actuator capability becomes less important with a larger the total work per cycle. Bottom: Micrographs showing source of required work: adhesive wedges deforming under load.

where  $m_r$  is the mass of the robot in kg. For example, if an ant has a normalized performance of 100, then it can drag 100 times its weight.

Figure 5 shows a range of measured coefficients of friction with corresponding normalized performances. A  $1 \text{ kg}$  machined stainless steel lab weight was used to measure coefficients of friction. Normalized performance was measured using a  $25 \text{ mm}$  square robot weighing  $12 \text{ g}$  with controllable adhesive on the bottom.

Note that the results are not strictly correlated with the coefficients of friction. Teflon (a) and powder-coated steel (b) have very different adhesive performances yet similar coefficients of friction. Teflon and polished concrete (c) have similar normalized payload performances but substantially different friction.

Glass has a very low coefficient of friction for steel, and provides the highest measured adhesive performance for these adhesives. This combination predicts that a  $12 \text{ g}$ ,  $25 \text{ mm}$  robot can move a payload over three thousand times its weight. If an adhesive robot system design chooses one material on which to operate, these common, low cost, smooth surfaces are a good choice. As seen in Fig. 5, the adhesive system is flexible. Although performance is excellent on glass, the system maintains good performance on a variety of surfaces.

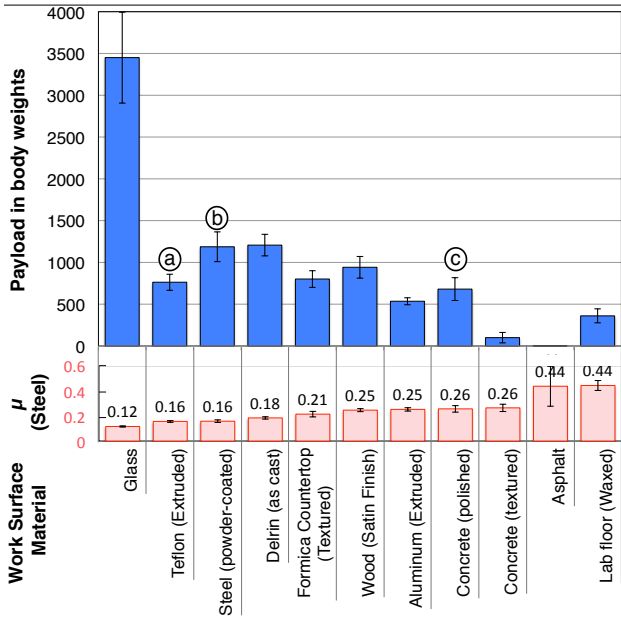


Fig. 5: Effective dragging payload capacity (in robot body weights) for a 12 g, 25 mm cube robot on a variety of surfaces sorted by coefficient of friction (also shown for reference).

### B. Actuator Selection

For the 25 mm square robot discussed, the actuator will need to produce 2 mJ of work per cycle at minimum. There is an additional requirement that the shape of the force-displacement curve be compatible with the adhesive system. Fully engaging the adhesive requires a motion of 100  $\mu\text{m}$ , and so the actuator must be capable at least this displacement for full use.

Solid state actuators are an attractive candidate for actuation of small robots as they are comparatively easy to manufacture at small sizes. Table I summarizes some common actuators, including available solid state ones, and the effect of these requirements for the proposed robot.

These force and displacement requirements make the most common solid state actuators difficult to use. Piezoelectric materials, particularly PZT, have high power densities but achieve these powers largely by performing many low-work cycles per second. This means there will have to be a lot of piezoelectric material in the robot to meet the work cycle constraint. Secondly, without some form of mechanical amplification, the displacements are small ( $\approx 300$  ppm) but with large force. This is poorly matched to the force-displacement curves of the adhesive. The basic bimorph design amplifies the motion at the expense of force making it more practical [22]. Further mechanical amplification is certainly possible [5], but adds complexity and extra compliance that must be overcome. In addition the resonant frequency of the actuator is reduced by adding mass at the extents, reducing the effective cycle rate.

Finally the shape of the force-displacement curve is reversed for many of these solid state actuators. Unlike the adhesive wedges, they make peak force at zero displacement

	Cycle Work (J/kg)	Volume Fraction for 25mm Cube Robot	Cycle Rate	Actuator Efficiency	Notes
Piezoelectric Bimorph (PZT)	2 J/kg	54% (w/o power supply)	Very High	10% - 30%	100s of Volts
Dielectric Elastomer (DE)	40 J/kg	2.4% (w/o power supply)	High	60% - 90%	1000s of Volts
Shape Memory Alloy Wire (Nitinol)	466 J/kg	0.012% (w/o large battery)	Slow	< 5%	large battery required
Servo Motor and Gearbox (HS-35HD)	Undefined (Gearing)	14%	Undefined (Gearing)	$\sim 20\%$	Minimal accessories required

TABLE I: Work cycles per actuation stroke of a variety of state of the art actuators (Data from [22]–[24] with a review found in [25]).

and zero force at maximum displacement. Piezoelectric and dielectric elastomer actuators both have this characteristic shape. This mismatch increases the effective actuator work by a factor of 4 for this class of actuators (Fig. 4c).

Shape memory alloy (Fig. 4d) is a good choice for both its high cycle work and good displacement matching to the adhesive system. Its relatively low speed however will not take advantage of the adhesive system’s speed capabilities, and its poor efficiency will require large batteries and high current drivers for practical use.

If the robot is large enough to use small electromagnetic or piezoelectric [26] motors and gearboxes, there are some potential advantages. A possible increase in efficiency compared to SMA, and a force profile tunable through gearing, present an opportunity to bypass some of the previously discussed constraints. Even if the engagement and disengagement of the adhesives represents a tiny amount of energy per cycle, this energy is also a fixed loss. It is therefore preferable for the sake of efficiency to take as large a stroke as possible rather than simply meeting these minimum requirements for locomotion. A continuously rotating actuator allows near arbitrarily large work cycles as shown in Fig. 4e.

We can derive an expression for the efficiency of a robot using these adhesives as follows:

$$\eta = \begin{cases} 0 & \text{if } \delta \leq \delta^* \\ \frac{\int_{\delta^*}^{\delta} f d\delta}{\int_0^{\delta^*} f d\delta + \int_{\delta^*}^{\delta} f d\delta} & \text{if } \delta > \delta^* \end{cases} \quad (3)$$

where  $\delta$  is the step size,  $\delta^*$  is the displacement required to load the adhesives (as defined in Fig. 4), and  $f$  is the force applied by the actuator.

Assuming a linear force profile for the adhesives, and assuming the actuator capable of matching the force profile, we can simplify this expression to the maximum efficiency of a robot using these adhesives:

$$\eta_{\max} = \begin{cases} 0 & \text{if } \delta \leq \delta^* \\ \frac{\delta - \delta^*}{\delta - \frac{1}{2}\delta^*} & \text{if } \delta > \delta^* \end{cases} \quad (4)$$

where  $\eta_{\max}$  is the maximum efficiency possible due to

	Commercial Walking Robot "Hexbug"	Winched $\mu$ Tug	SMA $\mu$ Tug	Piezo $\mu$ Tug
Length	50 mm	25 mm	150 mm w/Tail	32 mm
Width	60 mm	35 mm	25 mm	32 mm
Height	30 mm	25 mm	20 mm	20 mm
Mass	12.8 g	13.7 g	13 g	4.9 g
Max Tow Force	0.09 N	45 N	20 N	0.06 N
Step Rate	5 Hz	0.2 - 2 Hz	~0.5 Hz	30 Hz
Step Size	5 mm	5 - 20 mm	2 mm	0.4 mm

TABLE II: Comparison of demonstration robots presented in this paper to a simple commercially available robot.

adhesive loading. Naturally, there will be additional spring losses as well as other inefficiencies in any real system.

A robot that moves its payload  $100\ \mu\text{m}$  while requiring the full  $100\ \mu\text{m}$  of adhesive engagement will be at most 66% efficient. A locomotion efficiency of 90% is only theoretically possible with a step size  $\geq 450\ \mu\text{m}$  given these adhesives. This motivates building a robot capable of taking large steps ( $\delta \gg \delta^*$ ), i.e. a motor-based robot. As the load decreases,  $\delta^*$  decreases, so lightly loaded adhesives will also be more efficient for a given step size.

#### IV. RESULTS

A variety of robots were constructed to explore different features of the  $\mu$ Tugs concept. The commercially available "Hexbug" (Innovation First, Inc.<sup>1</sup>) hexapod walking robot was tested to provide a point of reference. Detailed specifications for each robot can be found in Table II.

##### A. Speed (Piezoelectric)

To show the speed capabilities of the adhesive system, a simple walking robot was constructed as seen in Fig. 6. Actuation of the legs is provided by two piezoelectric bimorphs (Steminc<sup>2</sup>) activated with a  $\pm 100\ \text{V}$  peak applied voltage. Actuating them with sinusoids phased by 90 degrees results in a semicircular trajectory at alternating pairs of legs, moving the robot forward. The robot was able to take light steps up to about 50 Hz. Maximum step size was  $500\ \mu\text{m}$ , but the stiffness and force output of the actuators limited performance, resulting in shorter steps at higher loads. Peak towing performance was obtained operating at 10 Hz, with the robot dragging 56 g or 10 times its body mass on glass. This result was limited by the force and displacement available from the actuators as well as their stiffness, not the limits of the adhesive which could achieve an order of magnitude larger shear adhesion.

##### B. Force / Work (SMA)

To better test the force capabilities of the adhesive, an inchworm robot was constructed using SMA as the actuator

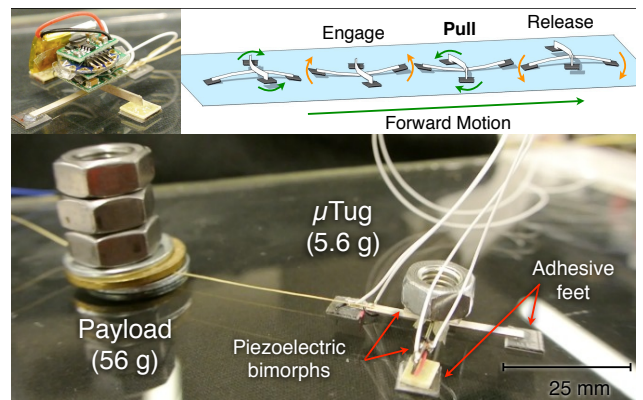


Fig. 6: Prototype of a piezo-based walker with a 5.6 g mass (including dummy electronic/battery payload) dragging 56 g on glass while taking 15 steps per second. The ultimate limit was found to be the actuator stiffness and work generating ability, not a lack of ability to achieve ground reaction force.

(Fig. 7). The impressive cycle work capabilities of SMA allowed the robot to generate more than 10 N of force with a maximum displacement of 2 mm. The robot was shown to easily drag 2.5 kg on glass, or over 500 times its body mass.

While this robot demonstrates the feasibility of full adhesive force capability at this scale, the weaknesses of SMA are also apparent. The robot could only move at a 0.5 Hz step rate, with a step size of about 3 mm, and was about 0.02% efficient due to the inherently low efficiency of SMA, poor control, and gait inefficiencies.

Dielectric elastomer actuators as shown in Table I can feasibly achieve the work cycles necessary to drive a robot this size and are an attractive option from a speed and efficiency standpoint. However, the required kilovolt power supply is larger and more complicated than the motor driver used for an SMA system. As power electronics improve dielectric elastomer actuators might become a better option in the future.

##### C. Unlimited Cycle Work (Motor)

While the piezoelectric and SMA robots demonstrated important elements of the feasibility of this concept, and both actuator types are well suited to scale to even smaller devices, they are not ideally suited to robots of this size. At length scales near 25 mm, electric motors are an available option; as discussed in Section III-B, they have advantages in efficiency and step size.

The use of a continuous-rotation actuator allows the output work cycle to be very large by extending the stroke; the design presented uses a winch, and so the work cycle is limited only by the length of the winch cable. The power density of the motor is much better than SMA, and its implementation requires no complicated electronics like EPAMs or piezoelectrics. A continuous-rotation actuator also permits use of a gearbox to match the motor output to the required adhesive work.

For this robot, we used a modified commercially available servo as the motor and gearbox. As shown in Fig. 8 below,

<sup>1</sup>www.hexbug.com

<sup>2</sup>www.steminc.com

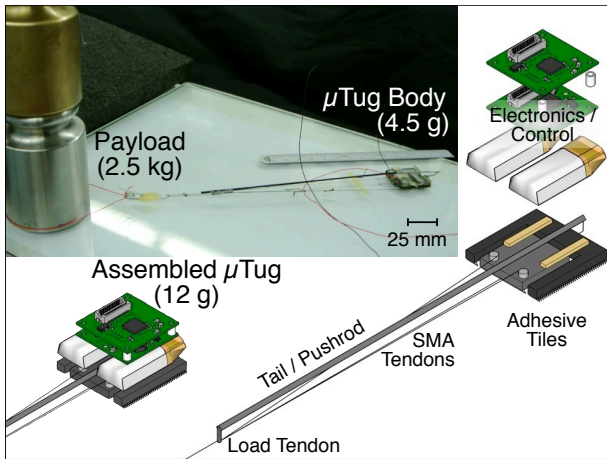


Fig. 7: Prototype of an SMA walker weighing 4.5 g (without onboard power) moving more than 2.5 kg horizontally on glass. The higher usable work per stroke of the SMA contributed to the substantially larger payload compared to the piezoelectric prototype.

the bulk of the robot consists of the servo as a winch, with a lift arm attached to its output through a friction clutch. The whole assembly sits on a solid 25 mm by 25 mm controllable adhesive tile. The clutch is designed so that when the winch is not tensioning the tow cable, the lift arm is lowered, allowing the two small drive motors to propel the robot. This gives the robot good mobility in both straight lines (6 body lengths per second) and turning (200 deg/sec) on the smooth surfaces it is designed for (see accompanying video for illustration).

When the robot tows a payload, the winch starts winding the tow cable, which lifts the arm that holds the drive wheels through the friction clutch. This drops the adhesive tile to the ground, allowing it to load. After a completed stroke, the winch reverses and releases the shear force on the adhesive tile; this drops the drive wheels and lifts the adhesive tile off of the surface. The drive wheels and motors maintain slight tension in the tow line while the winch unwinds, advancing the robot in preparation for another winch cycle.

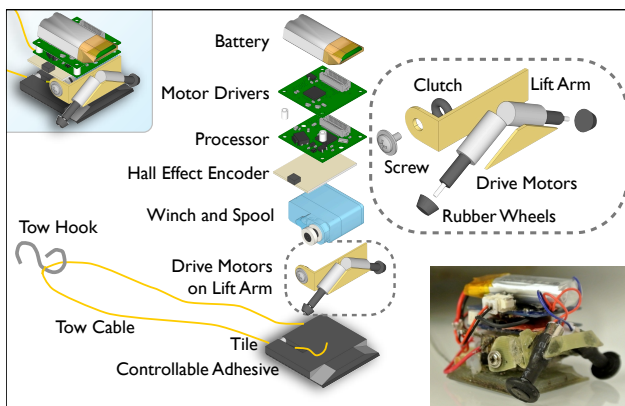


Fig. 8: Explosion view of the motor based  $\mu$ Tug demonstration robot.

This scheme trading contact from tile to wheels doubles the towing capability compared to inchworm designs of comparable size (see Section IV-B) by using all of the adhesive area at once. It relies on static friction being sufficient to keep the payload from moving between pulling strokes.

The ground reaction force measured from a single pulling step of the motor based  $\mu$ Tug is shown in Fig. 9 (top). The test was performed by towing 22.5 kg of painted, cast iron weights on glass. The  $\mu$ Tug was programmed to take a short step that moved the weight about 1 mm, and the resulting ground reaction forces were measured with a 6-axis ATI Gamma F/T sensor sampled at 500 Hz.

The peak shear force generated was just over 38 N or about 80% of the peak load predicted from adhesive testing, which corresponds to a normalized performance of 1875 as defined in (2). Note that although an effort was made to pull the weight as close to horizontally as possible, the normal ground reaction force was 3 N in the upwards direction. This is an adhesive normal force of over 50 times the robot's body weight. While this would clearly be impossible in a friction based system, it proved no trouble for the controllable adhesive system.

The same setup was used to pull the weight with a variety of step sizes and find the power consumed by the actuator in the process. The current was measured using a shunt resistor, sampling at 100 Hz, and the distance was measured using a dial test indicator with a resolution of about 10 microns. The results shown in Fig. 9 (bottom) demonstrate the efficiency increases with increased step size up to about 4 mm where the efficiency levels off to about 8%. This is dramatically more than the efficiency figures for either the piezoelectric or SMA  $\mu$ Tugs. The 4 mm step size is much larger than any length scale of the adhesives, indicating that the adhesives themselves are not the major source of compliance in this particular robot, which is probably dominated by the spring constant of the gears in the gearbox.

## V. CONCLUSION

Controllable adhesives make it possible to exert very large interaction forces in comparison to body weight and friction. However, they necessarily consume a certain amount of work and require a certain amount of time to engage and disengage with each loading cycle. In general, taking fewer and longer cycles or steps to cover a given distance is desirable, although this is increasingly difficult to do at small scales. For a given robot size, these considerations favor certain types of actuators over others.

For example, piezoelectric actuators may have difficulty achieving a sufficiently long stroke to engage and disengage the adhesive with each cycle. Walking with many small steps is possible, but reduces speed and efficiency. SMA actuators have a force-displacement profile that is well matched to the needs of controllable directional adhesives, can be very small, and can produce robots with very high interaction forces. However the speed and efficiency are low.

If the robot is large enough to use a continuously rotating motor (electromagnetic, piezoelectric or otherwise) and

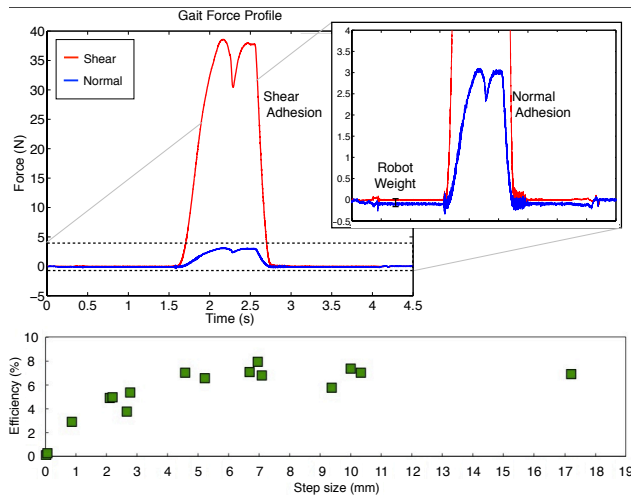


Fig. 9: Top: Measured ground reaction forces for the winched  $\mu$ Tug pulling 22.5 kg of weightlifting weights (or about two thousand times its weight) 1 mm on glass. Note the incidental normal force during the maneuver is equal to about 50 robot body weights in the upward direction, a feat only possible with adhesion. Bottom: The efficiency vs step size data for the same robot and setup. The efficiency reaches a steady state value of about 8% after a step size of 4 mm.

gearbox, the actuation cycle can be tailored to the needs of the adhesive for impressive performance. As expected, the efficiency increases with increasing step size due to the parasitic losses in the loading and unloading of the system including the adhesives as well as all other components that deform with such large loads.

As new adhesives with different engagement and disengagement characteristics are developed, these tradeoffs can be revisited. Piezoelectric actuator arrays or EPAM actuators may become attractive.

The performance of a  $\mu$ Tug also depends on the ratio of maximum adhesion to the coefficient of friction between the surface and the payload the robot is pulling. Glass is a particularly good material in this regard. For a motor-based  $\mu$ Tug it was possible to pull a payload greater than 1800 times the robot mass. This large ground reaction force capacity is still actuator limited, representing about 80% of the maximum load predicted by adhesive testing. Upon examination of the measured ground reaction forces, it is clear that this task could not be done with any sort of friction solution, as the ground reaction force shows the robot pulling up away from the ground with 50 body weights of force.

## VI. FUTURE WORK

Future improvements in performance will be possible if controllable directional adhesives can be optimized for a specific application, size range and set of surfaces. Given an actuator speed capability or chosen gait speed, an adhesive system should be optimized to minimize work and displacement while meeting the required speed.

Since the adhesives do not require normal force to work, and in fact produce adhesion under load, there is no reason

the same sort of small robot could not be designed to carry many times its body weight while climbing inclines or even vertical surfaces. In such applications, without the benefit of static friction holding the load in place between steps, some design changes will be needed to maintain line tension through the stepping cycle.

## ACKNOWLEDGMENT

The authors graciously thank Dr. T. Endlein for allowing the use of his beautiful weaver ant picture in Fig. 1 (<http://www.endlein.org>). We also graciously thank E. Eason for the use of his images of the adhesive limit curve (Fig. 2) as well as the micrograph views of adhesives loading (Fig. 4), as well as all his stimulating discussions and general help.

This material is based upon work supported by the Defense Advanced Research Projects Agency (DARPA) under Contract No. HR0011-12-C-0040.

Disclaimer: Any opinions, findings and conclusions or recommendations expressed in this material are those of the author(s) and do not necessarily reflect the views of the Defense Advanced Research Projects Agency (DARPA).

This material is also supported by the National Science Foundation Graduate Research Fellowship (NSF GRF), as well as a Stanford SOE Fellowship.

## REFERENCES

- [1] K. B. Yesin, K. Vollmers, and B. J. Nelson, "Modeling and control of untethered biomicrobots in a fluidic environment using electromagnetic fields," *The International Journal of Robotics Research*, vol. 25, no. 5-6, pp. 527-536, 2006.
- [2] E. Diller, C. Pawashe, S. Floyd, and M. Sitti, "Assembly and disassembly of magnetic mobile micro-robots towards deterministic 2-d reconfigurable micro-systems," *The International Journal of Robotics Research*, p. 0278364911416140, 2011.
- [3] R. Pelrine, A. Wong-Foy, B. McCoy, D. Holeman, R. Mahoney, G. Myers, J. Herson, and T. Low, "Diamagnetically levitated robots: An approach to massively parallel robotic systems with unusual motion properties," in *Robotics and Automation (ICRA), 2012 IEEE International Conference on*, pp. 739-744, IEEE, 2012.
- [4] R. J. Linderman and V. M. Bright, "Nanometer precision positioning robots utilizing optimized scratch drive actuators," *Sensors and Actuators A: Physical*, vol. 91, no. 3, pp. 292-300, 2001.
- [5] A. T. Baisch and R. J. Wood, "Pop-up assembly of a quadrupedal ambulatory microrobot," in *Intelligent Robots and Systems (IROS), 2013 IEEE/RSJ International Conference on*, pp. 1518-1524, IEEE, 2013.
- [6] S. Hollar, A. Flynn, C. Bellew, and K. Pister, "Solar powered 10 mg silicon robot," in *Micro Electro Mechanical Systems, 2003. MEMS-03 Kyoto. IEEE The Sixteenth Annual International Conference on*, pp. 706-711, IEEE, 2003.
- [7] R. Murthy, A. Das, and D. O. Popa, "Arripede: A stick-slip micro crawler/conveyor robot constructed via 2 1/2d mems assembly," in *Intelligent Robots and Systems, 2008. IROS 2008. IEEE/RSJ International Conference on*, pp. 34-40, IEEE, 2008.
- [8] W. Federle, M. Riehle, A. S. Curtis, and R. J. Full, "An integrative study of insect adhesion: mechanics and wet adhesion of pretarsal pads in ants," *Integrative and Comparative Biology*, vol. 42, no. 6, pp. 1100-1106, 2002.
- [9] S. Gorb, M. Varenberg, A. Peressadko, and J. Tuma, "Biomimetic mushroom-shaped fibrillar adhesive microstructure," *Journal of The Royal Society Interface*, vol. 4, no. 13, pp. 271-275, 2007.
- [10] R. S. Fearing, "Survey of sticking effects for micro parts handling," in *Intelligent Robots and Systems 95. Human Robot Interaction and Cooperative Robots, Proceedings. 1995 IEEE/RSJ International Conference on*, vol. 2, pp. 212-217, IEEE, 1995.
- [11] W. M. Van Spengen, R. Puers, and I. De Wolf, "On the physics of stiction and its impact on the reliability of microstructures," *Journal of Adhesion Science and Technology*, vol. 17, no. 4, pp. 563-582, 2003.

- [12] W. Federle and T. Endlein, "Locomotion and adhesion: dynamic control of adhesive surface contact in ants," *Arthropod structure & development*, vol. 33, no. 1, pp. 67–75, 2004.
- [13] T. Endlein and W. Federle, "Walking on smooth or rough ground: passive control of pretarsal attachment in ants," *Journal of Comparative Physiology A*, vol. 194, no. 1, pp. 49–60, 2008.
- [14] P. Day, E. V. Eason, N. Esparza, D. Christensen, and M. Cutkosky, "Microwedge machining for the manufacture of directional dry adhesives," *Journal of Micro and Nano-Manufacturing*, vol. 1, no. 1, p. 011001, 2013.
- [15] A. Parness, D. Soto, N. Esparza, N. Gravish, M. Wilkinson, K. Autumn, and M. Cutkosky, "A microfabricated wedge-shaped adhesive array displaying gecko-like dynamic adhesion, directionality and long lifetime," *Journal of The Royal Society Interface*, pp. rsif-2009, 2009.
- [16] K. Autumn, M. Sitti, Y. A. Liang, A. M. Peattie, W. R. Hansen, S. Sponberg, T. W. Kenny, R. Fearing, J. N. Israelachvili, and R. J. Full, "Evidence for van der waals adhesion in gecko setae," *Proceedings of the National Academy of Sciences*, vol. 99, no. 19, pp. 12252–12256, 2002.
- [17] M. P. Murphy, B. Aksak, and M. Sitti, "Gecko-inspired directional and controllable adhesion," *Small*, vol. 5, no. 2, pp. 170–175, 2009.
- [18] H. E. Jeong, J.-K. Lee, H. N. Kim, S. H. Moon, and K. Y. Suh, "A nontransferring dry adhesive with hierarchical polymer nanohairs," *Proceedings of the National Academy of Sciences*, vol. 106, no. 14, pp. 5639–5644, 2009.
- [19] M.-W. Moon, T.-G. Cha, K.-R. Lee, A. Vaziri, and H.-Y. Kim, "Tilted janus polymer pillars," *Soft Matter*, vol. 6, no. 16, pp. 3924–3929, 2010.
- [20] K. Autumn, S. Hsieh, D. Dudek, J. Chen, C. Chitaphan, and R. Full, "Dynamics of geckos running vertically," *Journal of Experimental Biology*, vol. 209, no. 2, pp. 260–272, 2006.
- [21] B.-m. Z. Newby and M. K. Chaudhury, "Friction in adhesion," *Langmuir*, vol. 14, pp. 4865–4872, 1998.
- [22] R. Wood, E. Steltz, and R. Fearing, "Optimal energy density piezoelectric bending actuators," *Sensors and Actuators A: Physical*, vol. 119, no. 2, pp. 476–488, 2005.
- [23] R. E. Pelrine, R. D. Kornbluh, and J. P. Joseph, "Electrostriction of polymer dielectrics with compliant electrodes as a means of actuation," *Sensors and Actuators A: Physical*, vol. 64, no. 1, pp. 77–85, 1998.
- [24] D. Reynaerts and H. V. Brussel, "Design aspects of shape memory actuators," *Mechatronics*, vol. 8, no. 6, pp. 635–656, 1998.
- [25] M. Karpelson, G.-Y. Wei, and R. J. Wood, "A review of actuation and power electronics options for flapping-wing robotic insects," in *Robotics and Automation, 2008. ICRA 2008. IEEE International Conference on*, pp. 779–786, IEEE, 2008.
- [26] A. M. Flynn, L. S. Tavrow, S. F. Bart, R. A. Brooks, D. Ehrlich, K. Udayakumar, and L. E. Cross, "Piezoelectric micromotors for microrobots," *Microelectromechanical Systems, Journal of*, vol. 1, no. 1, pp. 44–51, 1992.